# Thermal stability of HVPE-grown (0001) α-Ga<sub>2</sub>O<sub>3</sub> on sapphire template under vacuum and atmospheric environments ΦΘ

Special Collection: Gallium Oxide Materials and Devices

Zhuoqun Wen 🗷 🗓 ; Kamruzzaman Khan 🗓 ; Kai Sun 🗓 ; Ruby Wellen; Yuichi Oshima 🗓 ; Elaheh Ahmadi 🗓



J. Vac. Sci. Technol. A 41, 043403 (2023) https://doi.org/10.1116/6.0002559





CrossMark





## Thermal stability of HVPE-grown (0001) $\alpha$ -Ga<sub>2</sub>O<sub>3</sub> on sapphire template under vacuum and

Cite as: J. Vac. Sci. Technol. A 41, 043403 (2023); doi: 10.1116/6.0002559 Submitted: 6 February 2023 · Accepted: 3 May 2023 · Published Online: 31 May 2023







Zhuoqun Wen,<sup>1,a)</sup> 🕟 Kamruzzaman Khan,<sup>1</sup> 🔟 Kai Sun,<sup>1</sup> 🕩 Ruby Wellen,<sup>2</sup> Yuichi Oshima,<sup>3</sup> 🕩 and Elaheh Ahmadi<sup>2,4</sup> (D

#### **AFFILIATIONS**

- Department of Materials Science and Engineering, University of Michigan, Ann Arbor, Michigan 48109
- $^2$ Department of Electrical Engineering and Computer Science, University of Michigan, Ann Arbor, Michigan 48109
- <sup>3</sup>Optical Single Crystals Group, National Institute for Materials Science, Tsukuba 3050044, Japan

Note: This paper is part of the Special Topic Collection on Gallium Oxide Materials and Devices.

a)Author to whom correspondence should be addressed: wzhuogun@umich.edu

ABSTRACT

In the present study, thermal stability of  $\alpha$ -Ga<sub>2</sub>O<sub>3</sub> under vacuum and ambient pressure conditions was investigated *in situ* by x-ray diffraction and transmission electron microscopy (TEM). It was observed that the thermal stability of  $\alpha$ -Ga<sub>2</sub>O<sub>3</sub> increased by 200 °C when pressure was  $\frac{6}{8}$ lowered from an atmospheric to a vacuum level. This finding can be explained by oxygen diffusion under different oxygen partial pressures. In addition, in situ TEM imaging revealed that, once past the decomposition temperature, the onset of phase change propagates from the top crystal surface and accumulates strain, eventually resulting in a fractural film. The mechanism of α-Ga<sub>2</sub>O<sub>3</sub> to β-Ga<sub>2</sub>O<sub>3</sub> transition is evaluated through experiments and is discussed in this manuscript.

Published under an exclusive license by the AVS. https://doi.org/10.1116/6.0002559

#### I. INTRODUCTION

In the last few years, Ga<sub>2</sub>O<sub>3</sub> has gained tremendous interest for its potential applications in high-power switching and optoelectronics. More specifically, Ga2O3 can be used for detection in smaller wavelengths, such as solar blind deep-UV detectors, due to its ultrawide bandgap (Eg ranging from 4.7 to 5.3 eV). 1-7 Ga2O3 can be found in five common polymorph structures:  $\alpha$ ,  $\beta$ ,  $\gamma$ ,  $\epsilon$  (or  $\kappa$ ), and  $\delta$ . In particular, β-Ga<sub>2</sub>O<sub>3</sub>, which has a monoclinic crystal structure, has been studied extensively as it is the most thermodynamically stable phase. Nevertheless, recently, α-Ga<sub>2</sub>O<sub>3</sub> has gained considerable attention for its larger bandgap, at about 5.3 eV.  $^{10}$   $\alpha$ -Ga $_2$ O $_3$  also benefits from a corundum-like structure, similar to that of  $\alpha$ -Al<sub>2</sub>O<sub>3</sub>. This similarity in crystal structure suggests that the single crystalline growth of α-Ga<sub>2</sub>O<sub>3</sub> on inexpensive sapphire substrates can be achieved through standard techniques such as mist chemical vapor deposition, 10,12,13 pulsed laser deposition, 14 and halide vapor phase epitaxy (HVPE). 15 Remarkably, Oshima et al. have already succeeded

in demonstrating the HVPE growth of high-quality α-Ga<sub>2</sub>O<sub>3</sub> thin films on (0001) sapphire substrates with a high growth rate of  $150 \,\mu\text{m/h}$ .

With β-Ga<sub>2</sub>O<sub>3</sub> exhibiting the most stable polymorph, all metastable phases of Ga<sub>2</sub>O<sub>3</sub> eventually transit to the β-phase when exposed to high temperatures. Avoiding this phase change is crucial to maintaining the desired bandgap for a Ga<sub>2</sub>O<sub>3</sub> device and, thus, can be problematic for high-power applications, where temperature fluctuations are inevitable. In order to use the wide bandgap α-phase for such applications, extensive investigation is required to better understand the transition behavior of Ga<sub>2</sub>O<sub>3</sub> under various environmental conditions. One recent study conducted by Cora et al. characterized the dynamics of phase transition for the metastable κ-Ga<sub>2</sub>O<sub>3</sub> under both air and vacuum environments by in situ TEM. 16 It was found that for samples subjected to ambient atmospheric pressure, the κ-phase Ga<sub>2</sub>O<sub>3</sub> transitioned to an intermediate γ-phase before ultimately transitioning to the β-phase.

<sup>&</sup>lt;sup>4</sup>Applied Physics Program, University of Michigan, Ann Arbor, Michigan 48109



However, when under vacuum, κ-Ga<sub>2</sub>O<sub>3</sub> directly transformed into the β-phase structure without the occurrence of any intermediate phase transitions. Additionally, the temperature at which the phase transitions of κ-Ga<sub>2</sub>O<sub>3</sub> occurred was observed to be higher under vacuum levels compared to when exposed to atmospheric pressure.

Specifically, for α-Ga<sub>2</sub>O<sub>3</sub>, there are several studies evaluating the stability of α-Ga<sub>2</sub>O<sub>3</sub> at high temperatures for atmospheric pressure conditions. For example, recent studies on α-Ga<sub>2</sub>O<sub>3</sub> in atmospheric pressure demonstrated that the transition from α-Ga<sub>2</sub>O<sub>3</sub> to β-Ga<sub>2</sub>O<sub>3</sub> occurs at temperatures ranging from 600 to 650 °C. While another study revealed that α-Ga<sub>2</sub>O<sub>3</sub> can remain stable at temperatures as high as 800 °C if a selected-area growth method is used during the heteroepitaxial growth of Ga<sub>2</sub>O<sub>3</sub> on a sapphire substrate.<sup>18</sup> However, no research on the study of combined pressure and temperature effects on phase transformation has been conducted thus far. In the present study, the phase transition behavior of α-Ga<sub>2</sub>O<sub>3</sub> under atmospheric pressure and vacuum environments was assessed using in situ x-ray diffraction (XRD) and in situ TEM. And, with these results, a possible mechanism for  $\alpha$  to  $\beta$  phase transition is proposed.

#### II. EXPERIMENT

The two samples used for this study consisted of  $4 \mu m$  thick α-Ga<sub>2</sub>O<sub>3</sub> films grown on the (0001) sapphire substrate by HVPE under partial pressures p(HCl) = 0.25 kPa and  $p(O_2) = 1.0 \text{ kPa}$  at 550 °C. O2 and a mixture of GaCl and GaCl3 were used as precursors, while N2 was used as the carrier gas.20 Further details about the growth process can be found in Refs. 15 and 20.

An in situ XRD study of phase evolution for each α-Ga<sub>2</sub>O<sub>3</sub> film during ramping up the stage temperature was conducted with a Rigaku Smartlab XRD, using a Ge (220) × 2 monochromated Cu source. Two α-Ga<sub>2</sub>O<sub>3</sub> samples were examined in situ by XRD under both ambient and vacuum environments. XRD ω-2θ profiles were recorded at increments of 20 °C starting from 500 °C. Each sample was placed on an Anton Paar DHS1100 Domed Hot Stage with the temperature monitored by a thermocouple. These temperature-dependent measurements were performed both at atmospheric pressure and under vacuum. To achieve vacuum levels, a sample was sealed within the domed hot plate and pumped down to  $\sim 10^{-4}$  Torr. For both pressure conditions, the hot plate was first heated at a rate of 20 °C/min until reaching 500 °C. Next, the rate was reduced to 5 °C/min for target temperatures between 500 and 1000 °C. Each target temperature was allowed 5 min to stabilize before recording the XRD profile.

In situ TEM was also performed under similar conditions using a Thermo-Fisher TF30 TEM. The TEM measurements were all conducted under a vacuum environment, at  $\sim 10^{-7}$  Torr. A Thermo-Fisher Helios 650 Xe Plasma focused ion beam (FIB) system was used to prepare cross-sectional thin membrane specimens for TEM. The FIB liftouts were then transferred to DENSSolution nanochips and were subsequently mounted onto a DENSSolutions Wildfire double-tilt heating holder. The temperature of the holder was controlled using Impulse software. For the low-pressure environment, a sample was first heated to 400 °C using a ramp rate of 20 °C/min. The rate was then reduced to 5 °C/min for target temperatures higher than 400 °C. TEM bright-field (BF) images and

selected-area electron diffraction (SAED) patterns were recorded for each 50 °C interval until the α-Ga<sub>2</sub>O<sub>3</sub> sample visibly transformed into β-Ga<sub>2</sub>O<sub>3</sub>. The same TEM experiment at atmospheric pressure was also conducted using the same DENSSolution holder. However, this time the sample was first heated outside of the TEM chamber under an ambient environment from room temperature to 400 °C at the same rate of 20 °C/min. After this initial thermal treatment, the sample was transferred into the TEM chamber for immediate TEM BF and SAED imaging. During the whole process, the sample temperature was maintained by the heating holder. The sample and the heating holder were then taken out of the TEM chamber for heating up to the next target temperature under ambient environment. Similar to the experiments under high vacuum, the sample was observed by TEM for 50 °C increments, starting from 400 °C until α-Ga<sub>2</sub>O<sub>3</sub> fully transitioned to  $\beta\text{-}Ga_2O_3$  (Fig. 2). This is an example of a figure prepared for double-column publication. Cross-sectional scanning electron microscope (SEM) images of copper zinc tin sulfide films after annealing at (a) and (b) 600 °C, (c)-(e) 700 °C, and (f)-(h) 800 °C for (c) and (f) 30 min, (a), (d), and (g) 1h, and (b), (e), and (h) 2h. All scale bars are  $1 \mu m$ .

#### **III. RESULTS AND OBSERVATIONS**

#### A. In situ XRD experiments

The  $\alpha$  to  $\beta$  phase transitions under both environments were found to occur at 500 and 700 °C, respectively, in our in situ XRD experiments. The XRD  $\omega$ -2 $\theta$  profiles are shown in Fig. 1.

As seen in Fig. 1(a), the  $\omega$ -2 $\theta$  profiles for atmospheric conditions remained consistent with that of pure  $\alpha$ -Ga<sub>2</sub>O<sub>3</sub> for tempera-As seen in Fig. 1(a), the  $\omega$ -2 $\theta$  profiles for atmospheric conditures up to 500 °C. At 500 °C,  $\beta$ -Ga<sub>2</sub>O<sub>3</sub> 401 diffraction peak started to occur. A  $\beta$ -Ga<sub>2</sub>O<sub>3</sub>  $\bar{4}11$  diffraction peak can be observed in  $\omega$ -20  $\bar{4}$ scan at 520 °C, indicating the start of the α-Ga<sub>2</sub>O<sub>3</sub> to β-Ga<sub>2</sub>O<sub>3</sub> Ξ phase transition. It can also be seen that the  $\alpha\text{-Ga}_2\text{O}_3$  0006 peak  $\vec{\xi}$ intensity reduces at these higher temperatures. For the 540 °C profile, additional  $\beta$ -Ga<sub>2</sub>O<sub>3</sub> 202 and  $\bar{1}11$  peaks can also be seen in the XRD profile, with the β-Ga<sub>2</sub>O<sub>3</sub> 411 peak appearing more prominent. For the 560 °C profile, the α-Ga<sub>2</sub>O<sub>3</sub> 0006 peak can no longer be seen. Lastly, for temperatures up to 1000 °C, the XRD profile remains the same. After this final temperature had been reached, another  $\omega\text{--}2\theta$  profile was performed after the sample had cooled down to room temperature. This XRD profile still exhibits a β-Ga<sub>2</sub>O<sub>3</sub> peak profile, confirming the permanence of the α-Ga<sub>2</sub>O<sub>3</sub> to  $\beta$ -Ga<sub>2</sub>O<sub>3</sub> phase transition.

On the contrary, the XRD  $\omega$ -2 $\theta$  profiles measured under vacuum are fixed for temperatures from 20 to 680 °C [Fig. 1(b)]. As seen in the 700 °C profile, the  $\beta$ -Ga<sub>2</sub>O<sub>3</sub> 401 peak is visible and the α-Ga<sub>2</sub>O<sub>3</sub> 0006 peak intensity is noticeably reduced. For the 720 °C curve profile, the β-Ga<sub>2</sub>O<sub>3</sub> 411 is also observed and appears to increase in intensity for the 740 °C profile. Once above 720 °C, the α-Ga<sub>2</sub>O<sub>3</sub> peak is no longer visible. Once again, the XRD profile remains unchanged up to 1000 °C. From these data, it can be concluded that the phase transition from α-Ga<sub>2</sub>O<sub>3</sub> to β-Ga<sub>2</sub>O<sub>3</sub> begins at a much higher temperature, around 200 °C higher, for samples under vacuum environments compared to those heated in the atmosphere. The reasons for this increase in the thermal stability of α-Ga<sub>2</sub>O<sub>3</sub>, when under vacuum, will be addressed in detail in Sec. IV.

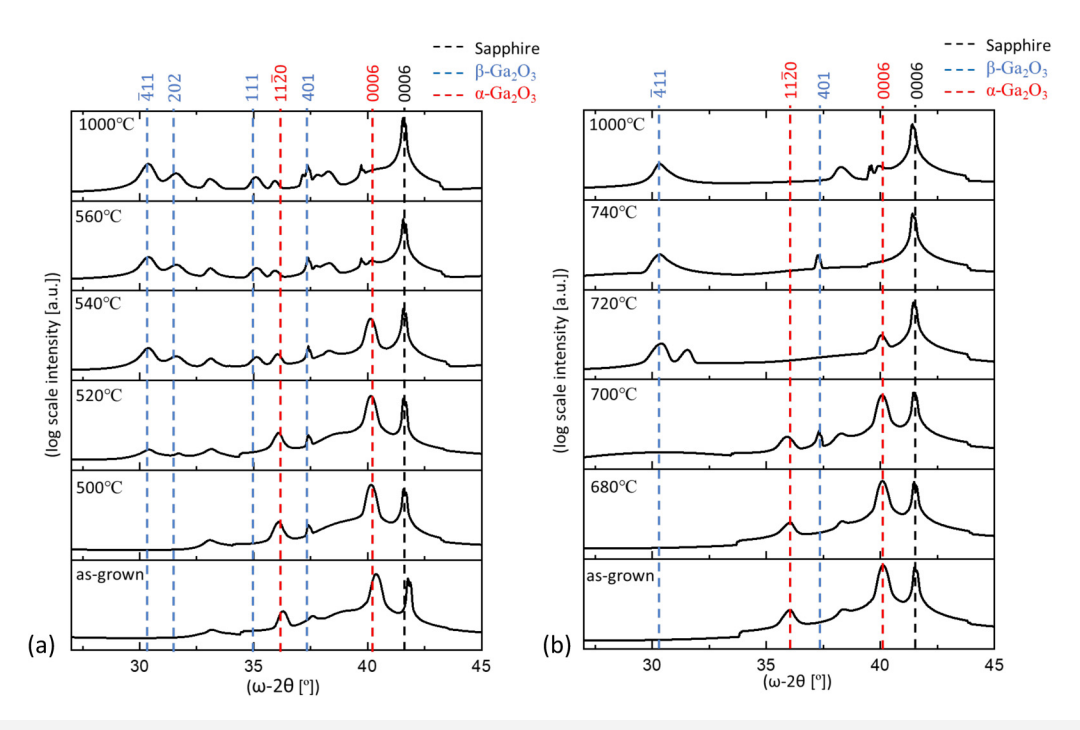
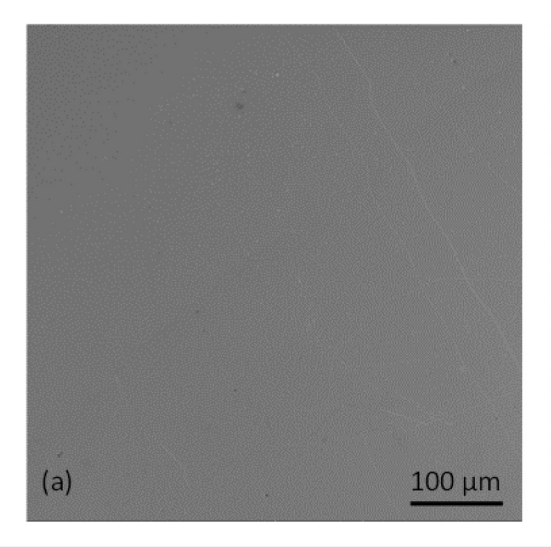


FIG. 1. XRD ω-2θ profiles collected at different temperatures. (a) In situ XRD patterns collected from the sample heated at atmospheric pressure. (b) In situ XRD patterns collected from  $\alpha$ -Ga<sub>2</sub>O<sub>3</sub> heated under vacuum. Red dashed lines designate the  $\alpha$ -Ga<sub>2</sub>O<sub>3</sub> peaks, and the blue dashed lines point to the  $\beta$ -Ga<sub>2</sub>O<sub>3</sub> peaks. The black dashed lines represent the location for the sapphire substrate for both XRD series.

Figure 2 shows SEM images of the α-Ga<sub>2</sub>O<sub>3</sub> sample before and after ramping up the temperature during the in situ XRD heating measurements under the atmosphere. Figure 2(a) presents an as-grown α-Ga<sub>2</sub>O<sub>3</sub> sample, which has a smooth and clear surface.

After the sample was heated to 560 °C during the in situ XRD  $_{22}^{82}$  measurements, the sample surface fractured. As discussed earlier, the sample fully transformed into  $\beta\text{-}Ga_2O_3$  at this temperature [Fig. 2(b)].



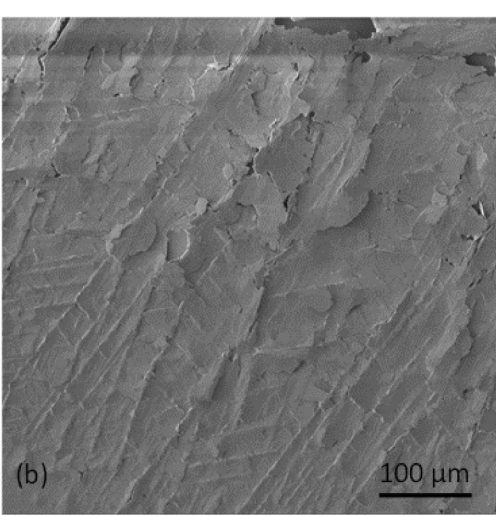


FIG. 2. (a) SEM image of the as-grown α-Ga<sub>2</sub>O<sub>3</sub> surface before heating experiment. (b) SEM image of the sample surface after heating experiment under atmosphere.



#### B. In situ TEM experiments

Figure 3 shows the TEM results of the experiment performed under atmospheric conditions. Figures 3(a) and 3(b) show the TEM BF image of the as-grown α-Ga<sub>2</sub>O<sub>3</sub> and SAED pattern at room temperature, taken from the sample along its [1011] zone axis, respectively. As seen from the TEM BF image, the α-Ga<sub>2</sub>O<sub>3</sub> sample has a high dislocation density. The SAED patterns remained unchanged ramping temperatures up to 600 °C. Once the temperature reached 600 °C, new spots became visible in the SAED pattern, aside from those from  $\alpha$ -Ga<sub>2</sub>O<sub>3</sub> [Fig. 3(f)], meaning β-Ga<sub>2</sub>O<sub>3</sub> began to appear. Additionally, dislocations disappeared partially at this temperature. After the temperature was increased to 700 °C, again, more diffraction spots became visible, as seen in Fig. 3(h). The  $4\mu$ m membrane specimen fractured when the temperature was raised to 750 °C [Fig. 3(i)]. The SAED pattern taken from this fractured film [Fig. 3(j)] confirmed that the  $\alpha$ -Ga<sub>2</sub>O<sub>3</sub> phase fully transformed into β-Ga<sub>2</sub>O<sub>3</sub>, which was the same as the SEM observations after XRD experiments.

Figure 4 shows the results of in situ TEM experiments under vacuum. The SAED patterns [Figs. 4(b) and 4(d)] suggest that the α-Ga<sub>2</sub>O<sub>3</sub> phase remained stable up to 700 °C. TEM BF images [Figs. 4(a), 4(c), and 4(e)] also reveal that the dislocation density reduced with increasing temperature. The phase transition began at 800 °C, where points  $\bar{2}00_{\beta}$  and  $\bar{3}10_{\beta}$  can be seen in the diffraction pattern [Fig. 4(f)]. At 850 °C, the sample fractured [Fig. 4(j)] when it fully transformed into β-Ga<sub>2</sub>O<sub>3</sub>, as evident in the SAED [Fig. 4(h)]. The phase transformation under vacuum occurred at a higher temperature than that under ambient temperature. In addition, the phase transformation from  $\alpha\text{-Ga}_2O_3$  and  $\beta\text{-Ga}_2O_3$ during the TEM measurement happened at a higher temperature than that during the XRD measurement. These results will be discussed in detail in Sec. IV.

Figure 5 shows the in situ TEM diffraction patterns for different locations of the sample heated to 600 °C under atmospheric pressure. From these images, it can be concluded that the phase change began at the surface of the sample. Figure 5(a) shows that the zone axis of  $[001]_{\beta}$  occurred on the top surface, while the other areas of the sample consisted of only  $[10\overline{10}]_{\alpha}$  direction [Figs. 5(b)-5(c)]. Any other spots in the pattern besides  $[10\overline{1}0]_{\alpha}$ in Fig. 5(c) could be attributed to the  $[10\bar{1}0]$  zone axis of the sapphire substrate. Figures 5(e) and 5(f) show the crystal structures of  $\alpha$ -Ga<sub>2</sub>O<sub>3</sub> and  $\beta$ -Ga<sub>2</sub>O<sub>3</sub> aligned along the  $[10\bar{1}0]_{\alpha}$  and  $[001]_{\beta}$ directions, respectively.

Table I summarizes the experiments results of both TEM and XRD experiments in ambient and vacuum environments conducted at different temperatures.

#### **IV. DISCUSSIONS**

From the experiments above, we can conclude that α-Ga<sub>2</sub>O<sub>3</sub> to β-Ga<sub>2</sub>O<sub>3</sub> phase transition: (i) completes at dozens of degrees higher than the phase transition starts; (ii) starts at the surface of materials and results in fracturing the film; (iii) occurs at 100 °C lower by XRD measurements than that by TEM measurements under similar conditions; and (iv) occurs at ~200 °C higher under vacuum than that under ambient environment. It is reported that the phase transition temperature for  $\alpha$ -Ga<sub>2</sub>O<sub>3</sub> to  $\beta$ -Ga<sub>2</sub>O<sub>3</sub> under atmospheric pressure is between 600 and 650 °C. 17-19 α-Ga<sub>2</sub>O<sub>3</sub> to β-Ga<sub>2</sub>O<sub>3</sub> phase transition can be characterized as a pseudomartensitic transformation, which mainly involves two steps: (a) the repeated O sublattice transformation by shearing close-packed O layers and (b)  $\stackrel{\omega}{\sim}$ the periodical reordering of Ga.<sup>21,22</sup> Pseudomartensitic transformation is a multistep and multitype phase transition. In our case, several structurally ordered sublattices  $GaO_{x}$ , (x = 4, 5, and 6) are involved  $\frac{80}{2}$ during the transition. One feature of such transformation is that the

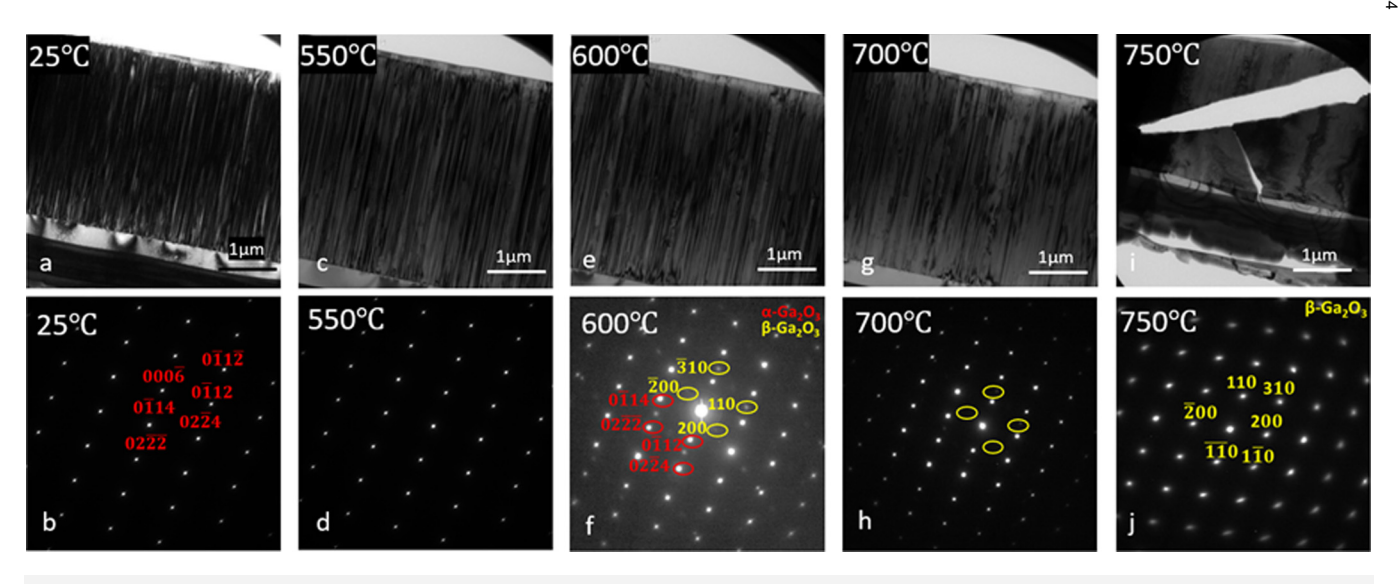
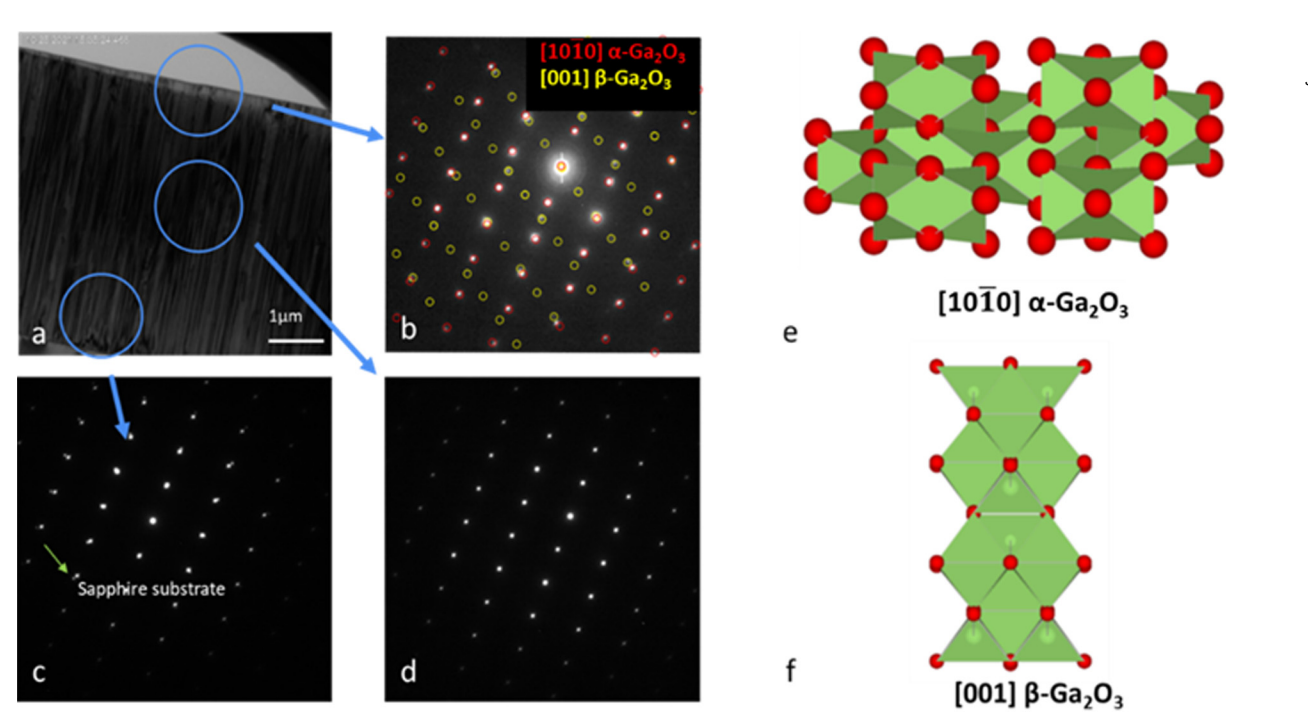


FIG. 3. In situ TEM analysis under ambient environment. BF images and SAED patterns from the Ga<sub>2</sub>O<sub>3</sub> layer at room temperature [(a)and (b)], at 550 °C [(c) and (d)], at 600 °C [(e) and (f)], at 700 °C [(g) and (h)], and at 750 °C [(i) and (j)], respectively. All BF images and SAED patterns were taken from the same region.

**FIG. 4.** In situ TEM analysis under a vacuum environment. BF image and SAED pattern from the  $Ga_2O_3$  layer at room temperature [(a) and (b)], at 700 °C [(c) and (d)], at 800 °C [(e) and (f)], and at 850 °C [(g) and (h)], respectively. All BF images and SAED patterns were taken from the same sample region.



**FIG. 5.** (a) Cross-sectional TEM BF image at 600 °C under ambient environment. The SAED patterns are taken from (b) the top surface of the sample, with [001]  $\beta$ -Ga<sub>2</sub>O<sub>3</sub> occurring alongside the original α-phase, (c) the bottom of the sample where the substrate diffraction pattern can be observed, and (d) the middle of the sample. Lastly, (e) and (f) are the crystal structures for the [1010]  $\alpha$  and [001]  $\beta$  directions.



TABLE I. List of samples for the experiments.

Sample No.	Experimental environment	Analysis method	Ramp rate	Scanning temperature	Phase transition temperature (°C)
1	Vacuum	XRD analysis	T ≤ 500 °C: 20 °C/min	Every 20 °C when T > 500 °C	680-700
2	Ambient	·	$T > 500  ^{\circ}\text{C}: 5  ^{\circ}\text{C/min}$		500-520
3	Vacuum	TEM analysis	$T \le 400$ °C: 20 °C/min	Every 50 °C when $T > 400$ °C	800
4	Ambient		T > 400 °C: 5 °C/min		600

phase transition is a slow process because of multitype reactions and the high energy barrier of atom reconstruction (1). This feature is observed in our experiments: after the first  $\beta$  occurrence, the  $\alpha$  to  $\beta$ phase transition was not completed until the samples were heated for more than 30 min and at higher temperatures. Jinno et al. hypothesize that the thermal stress in α-Ga<sub>2</sub>O<sub>3</sub> mainly contributes to the  $\alpha$  to  $\beta$  phase transition. They have pointed out that samples will bend under high temperatures due to the differences in the thermal expansion coefficients of sapphire and α-Ga<sub>2</sub>O<sub>3</sub> layer. 17,23,24 When bending, strain is induced and accumulated at the surface of the sample and stress is accumulated at the bottom of it. When approaching a critical temperature, the strain at the top of the thin film accumulates to an extent that can lead to a slip plane shift, which results in the start of  $\alpha$  to  $\beta$  phase transition.<sup>25</sup> Moreover, it is also known that the α-Ga<sub>2</sub>O<sub>3</sub> layer has in-plane compressive stress at the interface of the sapphire substrate due to the lattice mismatch.<sup>12</sup> Such compressive stress can partially compensate for the thermal stress and results in the bottom layer being more unlikely to start the phase transition than the top layer. It is also observed that the phase transition temperature is ~100 °C lower in XRD studies than in TEM studies in the same environment. This is because of the different sizes of the samples that were used for each experiment. Jinno et al. also reported that selective-area grown α-Ga<sub>2</sub>O<sub>3</sub> could enhance thermal stability due to reducing dislocation density and thermal stress in the window patterns (15). In our XRD experiments, a 2-in.  $\alpha$ -Ga<sub>2</sub>O<sub>3</sub> wafer was diced into  $10 \times 10 \text{ mm}^2$  square samples for the XRD measurements, whereas the TEM specimens were  $\sim$ 6  $\mu$ m wide,  $\sim$ 120 nm thick, and several micrometer long. During thermal treatments, thermal strain can be more released in the nanoscale specimen (those used for TEM studies) than the larger samples (those used for XRD studies), which results in the  $\alpha$  to  $\beta$ phase transition starting at a lower temperature than the TEM study specimen.

The higher thermal stability of α-Ga<sub>2</sub>O<sub>3</sub> under a vacuum environment may be due to the differences in O2 partial pressure (pO<sub>2</sub>). As mentioned above, O sublattice transformation and Ga reconstruction are the two elementary steps of  $\alpha$  to  $\beta$  phase transition. The higher coordination number of Ga-O intermediates such as  $(GaO_x, x = 4, 5, and 6)$  are formed during the phase transition.<sup>21</sup> The concentration of these high number O coordinated intermediates decreases under a low pO2 environment, which limits the O diffusion in Ga<sub>2</sub>O<sub>3</sub> and increases the overall energy barrier of the phase transition. 26,27 Compared to atmospheric environment ( $pO_2 = 0.21$  atm),  $pO_2$  is nearly zero under vacuum environment. As a result, the  $\alpha$  to  $\beta$  phase transition is more difficult under a vacuum environment, leading to a higher thermal stability of  $\alpha$ -Ga<sub>2</sub>O<sub>3</sub>.

#### V. SUMMARY AND CONCLUSIONS

Both in situ XRD and in situ TEM experiments revealed that the  $\alpha$ -Ga<sub>2</sub>O<sub>3</sub> to  $\beta$ -Ga<sub>2</sub>O<sub>3</sub> phase transition temperature increased by 200 °C under a high vacuum environment than under ambient conditions. This observation is explained by the impact of oxygen partial pressure on oxygen diffusion. The XRD results indicated that the large α-Ga<sub>2</sub>O<sub>3</sub> piece started to transform into β-Ga<sub>2</sub>O<sub>3</sub> at 500 and 700 °C under ambient and vacuum, respectively. The phase transition under both environments was completed at dozens of degree Celsius higher than the first occurrence of the  $\beta$   $_{\mbox{\scriptsize $\Theta$}}$ phase. Fractured films were observed under both SEM and TEM images after the  $\alpha$  to  $\beta$  phase transition completed. The *in situ*  $\frac{1}{2}$ TEM observations showed that the phase transition temperature for nanoscale  $\alpha$ -Ga<sub>2</sub>O<sub>3</sub> sample was 600 °C under ambient environments and 800 °C under high vacuum. In addition, TEM observations also revealed that with the increase in temperature, the  $\vec{\xi}$ dislocation density of  $\alpha$ -Ga<sub>2</sub>O<sub>3</sub> sample decreased and the  $\alpha$  to  $\beta$ phase transition started at the top surface. The result of the phase transition temperature is ~100 °C higher under TEM experiments than the temperature under XRD experiments, which can be explained by the difference in strain accumulation under different sizes of samples.

#### **ACKNOWLEDGMENTS**

This work was supported by the Air Force Office of Scientific Research (Program Manager, Dr. Ali Sayir) through Program FA9550-20-1-0045 and the National Science Foundation (NSF) under Grant No. 2043803. The authors also acknowledge the financial support of the University of Michigan College of Engineering for the Thermo-Fisher G4 650 Xe Plasma-FIB and TF30 in situ ion irradiation TEM.

### **AUTHOR DECLARATIONS Conflict of Interest**

The authors have no conflicts to disclose.



#### **Author Contributions**

Zhuoqun Wen: Conceptualization (equal); Data curation (equal); Formal analysis (equal); Investigation (equal); Methodology (equal); Writing - original draft (equal). Kamruzzaman Khan: Conceptualization (equal); Formal analysis (equal); Investigation (equal); Methodology (equal); Writing - review & editing (equal). Kai Sun: Data curation (equal); Formal analysis (equal); Investigation (equal); Methodology (equal). Ruby Wellen: Data curation (equal); Formal analysis (equal); Writing - original draft (equal). Yuichi Oshima: Data curation (equal); Formal analysis (equal); Investigation (equal); Methodology (equal); Writing review & editing (equal). Elaheh Ahmadi: Data curation (equal); Formal analysis (equal); Funding acquisition (lead); Methodology (equal); Resources (lead); Writing - review & editing (equal).

#### DATA AVAILABILITY

The data that support the findings of this study are available from the corresponding author upon reasonable request.

#### **REFERENCES**

- <sup>1</sup>S. J. Pearton, J. Yang, P. H. Cary IV, F. Ren, J. Kim, M. J. Tadjer, and M. A. Mastro, Appl. Phys. Rev. 5, 011301 (2018).
- <sup>2</sup>M. A. Mastro, A. Kuramata, J. Calkins, J. Kim, F. Ren, and S. Pearton, ECS J. Solid State Sci. Technol. 6, P356 (2017).
- <sup>3</sup>M. Higashiwaki, K. Sasaki, H. Murakami, Y. Kumagai, A. Koukitu, A. Kuramata, T. Masui, and S. Yamakoshi, Sci. Tech. 31, 034001 (2016).
- <sup>4</sup>K. Takahashi, A. Yoshikawa, and A. Sandhu, Wide Bandgap Semiconductors (Verlag Berlin, Heidelberg, 2007).
- <sup>5</sup>E. Ahmadi and Y. Oshima, J. Appl. Phys. 126, 160901 (2019).

- <sup>6</sup>Z. Wen, K. Khan, X. Zhai, and E. Ahmadi, Appl. Phys. Lett. 122, 082101
- <sup>7</sup>X. Xia et al., J. Vac. Sci. Technol. A **41**, 023205 (2023).
- <sup>8</sup>R. Roy, V. G. Hill, and E. F. Osborn, J. Am. Chem. Soc. 74, 719 (1952).
- <sup>9</sup>J. Åhman, G. Svensson, and J. Albertsson, Acta Crystallogr. C **52**, 1336 (1996). <sup>10</sup>D. Shinohara and S. Fujita, Jpn. J. Appl. Phys. **47**, 7311 (2008).
- <sup>11</sup>M. Marezio and J. P. Remeika, J. Chem. Phys. **46**, 1862 (1967).
- <sup>12</sup>K. Kaneko, H. Kawanowa, H. Ito, and S. Fujita, Jpn. J. Appl. Phys. 51, 020201
- <sup>13</sup>R. Jinno, T. Uchida, K. Kaneko, and S. Fujita, Appl. Phys. Express 9, 071101 (2016).
- <sup>14</sup>D. Y. Guo, X. L. Zhao, Y. S. Zhi, W. Cui, Y. Q. Huang, Y. H. An, P. G. Li, Z. P. Wu, and W. H. Tang, Mater. Lett. 164, 364 (2016).
- 15Y. Oshima, E. G. Villora, and K. Shimamura, Appl. Phys. Express 8, 055501 (2015).
- 16 I. Cora, Z. Fogarassy, R. Fornari, M. Bosi, A. Rečnik, and B. Pécz, Acta Mater. 183, 216 (2020).
- 17 R. Jinno, K. Kaneko, and S. Fujita, AIP Adv. 10, 115013 (2020).
- 18 J. P. McCandless et al., Appl. Phys. Lett. 119, 062102 (2021).
- <sup>19</sup>S. D. Lee, K. Akaiwa, and S. Fujita, Phys. Status Solidi C 10, 1592 (2013).
- 20 Y. Oshima, K. Kawara, T. Oshima, M. Okigawa, and T. Shinohe, Sci. Tech. 35, 055022 (2020).
- <sup>21</sup>S.-C. Zhu, S.-H. Guan, and Z.-P. Liu, Phys. Chem. Chem. Phys. 18, 18563
- <sup>22</sup>M. A. Fradkin, Phys. Rev. B 50, 16326 (1994).
- <sup>23</sup>W. M. Yim and R. J. Paff, J. Appl. Phys. **45**, 1456 (1974).
- <sup>24</sup>L. J. Eckert and R. C. Bradt, J. Am. Ceram. Soc. **56**, 229 (1973).
- **25**S. A. Rather and B. K. Saha, Cryst. Growth Des. **18**, 2712 (2018).
- <sup>26</sup>J. Lane and J. Kilner, Solid State Ionics 136–137, 997 (2000).
- 27 P.-M. Geffroy, L. Guironnet, H. J. M. Bouwmeester, T. Chartier, J.-C. Grenier, and J.-M. Bassat, J. Eur. Ceram. Soc. 39, 59 (2019).